Semiconductor Physics, Quantum Electronics & Optoelectronics, 2006. V. 9, N 4. P. 71-76.

PACS 84.40.Xb

Radar cross section study from wave scattering structures

S. Redadaa, A. Boualleg, N. Merabtine, and M. Benslama
Electromagnetism and Telecommunications Laboratory LET
Department of Electronics, Faculty of Engineering
University of Constantine, Algeria
E-mail: {redasdz, bouadzdz}@yahoo.fr; {na_merabtine, malekbenslama}@hotmail.com

Abstract. Radar remote sensing deals with the extraction of object information from electromagnetic wave parameters. To fully exploit the potential of acquiring quantitative information requires a detailed description of the microwaves scattering. The research on this topic was mostly centered on far-field analysis that assumes an incident plane wave, computation of its scattered field, and evaluation of the radar cross section. However, under certain practical conditions, the far-field analysis is not valid and a near-field analysis is necessary. In this paper, we have given a full analysis of the near-field of a wedge structure due to an incident wave field from a line source or a plane wave. The far-field pattern, for the case of a line source exciting the structure, is also analyzed.

Keywords: electromagnetic wave, scattering, structure, radar cross section.

Manuscript received 04.05.06; accepted for publication 23.10.06.

1. Introduction

The problem of electromagnetic wave scattering is very important in many applications, namely, remote sensing, antennas design and especially in defense applications. The research on this topic was mostly centered on far-field analysis that assumes an incident plane wave, computation of its scattered field due to the scatterer, and evaluation of the radar cross section (RCS) of the scatterer. When the transmitting and receiving antennas are far from the scatterer, the incident wave can be approximated by a plane wave and the scattered far-field can be regarded as the radiation far-field due to the induced currents on the scatterer, the far-field analysis thus applies. However, in practical applications, there are many situations, when the distance between the transmitting antenna and the scatterer is not large enough to treat the field arriving the scatterer as a plane wave, and the relative motion between the antennas and scatterer will produce the Doppler frequency shift. In these conditions, the far-field analysis is not valid and a near-field analysis is necessary [1].

In calculating the radar cross section of complex targets [2, 3], some parts of the structure can be modeled using singly curved sheets as, for example, the wings of an aircraft. For electrically large bodies, the geometrical theory of diffraction (GTD) [4, 5] is a good high frequency technique to compute the scattering from those bodies. But, as is well known, that method is not valid in the caustic of reflected rays, which occurs, for example, when we illuminate a singly curved screen with a plane wave. Physical optics (PO) has been largely used in the last years to predict high frequency radar cross section problems, because, unlike geometrical optics and the GTD, it is valid in the transition regions and at caustics. PO can be improved using the fringe currents contribution of the edge currents of the physical theory of diffraction (PTD) [6, 7].

This paper is organized as follows. Section 2 provides the scattering analysis; we present the RCS formulae and possible approximations. We calculate field expressions for the problem of scattering by a two-dimensional perfect electric conduction wedge capped with a dielectric cylinder. In Section 3, some numerical results for various configurations of the wedge structure are presented. Finally, a conclusion is given.

2. Scattering analysis

The RCS of a target characterizes its scattering property that is defined as the area intercepting the amount of power that, when scattered isotropically, produces in a receiver a density that is equal to the density scattered by the actual target. When the transmitter and receiver are in the same location, the RCS is referred to as mono-static (or backscattered), and it is referred to as bistatic when these two ones are located at different positions.

For three-dimensional target, the RCS is given in terms of incident power density, magnetic field, and electric field [8]**.** The RCS in terms of electric field is given by

$$\sigma_{3-D} = \lim_{\rho\to\infty}\left[4\pi\rho^2\frac{\left|E^s\right|^2}{\left|E^i\right|^2}\right], \tag{1}$$

where ρ is the distance from the target to observation point, E^s and E^i are the scattered and incident electric field. Eq. (1) is valid when the target is illuminated by a plane wave that in practice can be only approximated when the target is placed in the far-field of the source, at least $\rho = 2D^2/\lambda$, where D is the largest dimension of the target.

Consider a perfectly conducting rectangular thin-flat plate in the $x-y$ plane as shown in Fig. 1. For a linearly polarized incident wave in the $x-y$ plane, the horizontal and vertical backscattered RCSs are, respectively, given by

$$\sigma_V = \frac{b^2}{\pi}\left|\sigma_{1V} - \sigma_{2V}\left[\frac{1}{\cos\theta} + \frac{\sigma_{2V}}{4}\left(\sigma_{3V}+\sigma_{4V}\right)\sigma_{5V}^{-1}\right]\right|^2, \tag{2}$$

$$\sigma_H = \frac{b^2}{\pi}\left|\sigma_{1H} - \sigma_{2H}\left[\frac{1}{\cos\theta} - \frac{\sigma_{2H}}{4}\left(\sigma_{3H}+\sigma_{4H}\right)\sigma_{5H}^{-1}\right]\right|^2, \tag{3}$$

where

$$\begin{aligned}
&\sigma_{1V} = \cos\left(k_a\sin\theta\right) - j\frac{\sin\left(k_a\sin\theta\right)}{\sin\theta},\\
&\sigma_{2V} = \frac{e^{j(ka-\pi/4)}}{\sqrt{2\pi}\left(k_a\right)^{3/2}},\\
&\sigma_{3V} = \frac{\left(1+\sin\theta\right)e^{-jk_a\sin\theta}}{\left(1-\sin\theta\right)^2},\\
&\sigma_{4V} = \frac{\left(1-\sin\theta\right)e^{jk_a\sin\theta}}{\left(1+\sin\theta\right)^2},\\
&\sigma_{5V} = 1 - \frac{e^{j(2k_a-\pi/2)}}{8\pi\left(k_a\right)^3};
\end{aligned} \tag{4}$$

$$\begin{aligned}
&\sigma_{1H} = \left(\sigma_{1V}\right)^*,\\
&\sigma_{2H} = \frac{4\,e^{j(k_a+\pi/4)}}{\sqrt{2\pi}\left(k_a\right)^{1/2}},\\
&\sigma_{3H} = \frac{e^{-jk_a\sin\theta}}{1-\sin\theta},\quad \sigma_{4H} = \frac{e^{-jk_a\sin\theta}}{1-\sin\theta},\\
&\sigma_{5H} = 1 - \frac{e^{j(2k_a+\pi/2)}}{2\pi\left(k_a\right)}.
\end{aligned} \tag{5}$$

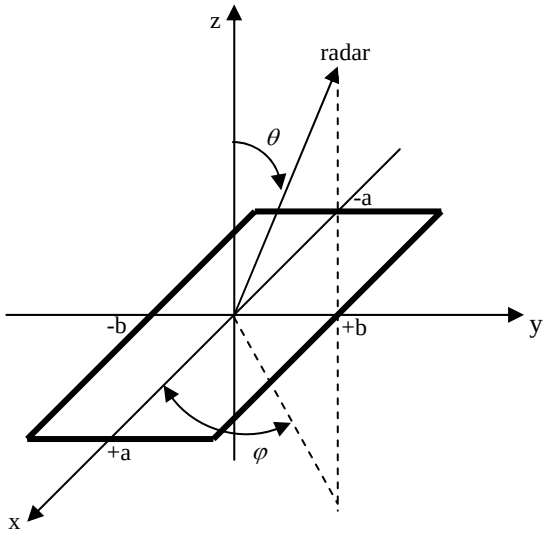

Fig. 1. Coordinates for the rectangular flat plate.

Here $k_a = k_0 a$, k_0 is the free space wave number. Eqs (2) and (3) are valid quite accurate for the aspect angles $0 \le \theta \le 80°$. For the aspect angles near 90°, Ross [9] obtained an empirical expression for the RCS by extensive fitting of measured data. It is given by

$\sigma_H \to 0$,

$$\sigma_V = \frac{a\,b}{\lambda}\left\{\left[1+\frac{\pi}{2\left(2a/\lambda\right)^2}\right] + \left[1-\frac{\pi}{2\left(2a/\lambda\right)^2}\right]\cos\left(2k_a - \frac{3\pi}{5}\right)\right\}. \tag{6}$$

The backscattered RCS for a perfectly conducting thin rectangular plate for incident waves at any θ, φ can be approximated by

$$\sigma = \frac{4\pi\,a^2b^2}{\lambda^2}\left(\frac{\sin\left(a\,k_0\sin\theta\cos\varphi\right)}{a\,k_0\sin\theta\cos\varphi}\times \frac{\sin\left(b\,k_0\sin\theta\cos\varphi\right)}{b\,k_0\sin\theta\cos\varphi}\right)^2\left(\cos\theta\right)^2. \tag{7}$$

Eq. (7) is independent of the polarization, and it is only valid for the aspect angles $\theta \le 20°$. Fig. 2 shows the backscattered RCS of a rectangular flat plate, for both vertical and horizontal polarizations.

The goal of analysis is to find the field expressions for the problem of scattering by a two-dimensional (2-D) perfect electric conduction (PEC) wedge capped with a dielectric cylinder as shown in Fig. 3. Using the cylindrical coordinates system, the excitation due to an electric line current of amplitude I_e located at (ρ_0, φ_0) result in transverse magnetic (TM) incident field with the electric field expression given by

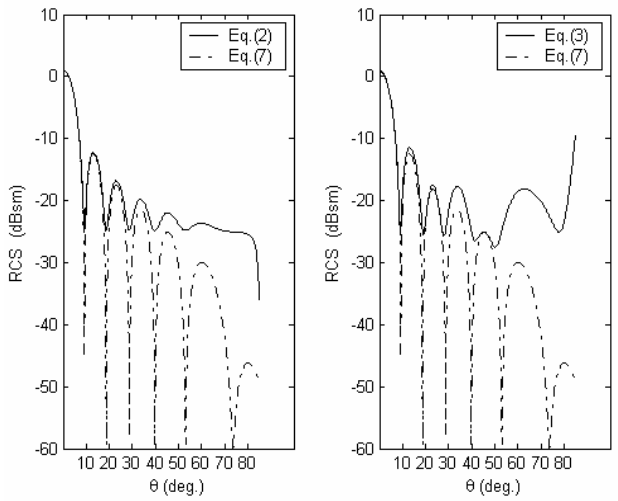

Fig. 2. Backscattered RCS for a rectangular flat plate of vertical (a) and horizontal (b) polarizations.

$$E_z^i = -I_e \frac{\omega \mu_0}{4} H_0^{(2)}\left(k_0 \left| \rho - \rho_0 \right|\right), \tag{8}$$

where $H_0^{(2)}$ is the Hankel function of the second kind of order zero.

The problem is divided into three regions I, II, and III. The field expressions may be assumed to take the following forms:

$$\begin{aligned} E_z^{\mathrm{I}} &= \sum_{n=0}^{\infty} a_n J_\nu(k_1\rho)\sin\nu(\varphi-\alpha)\sin\nu(\varphi_0-\alpha), \\ E_z^{\mathrm{II}} &= \\ &= \sum_{n=0}^{\infty}\left(b_n J_\nu(k_0\rho)+c_n H_\nu^{(2)}(k_0\rho)\right)\sin\nu(\varphi-\alpha)\sin\nu(\varphi_0-\alpha), \\ E_z^{\mathrm{III}} &= \sum_{n=0}^{\infty} d_n H_\nu^{(2)}(k_0\rho)\sin\nu(\varphi-\alpha)\sin\nu(\varphi_0-\alpha), \end{aligned} \tag{9}$$

where k_1 is the wave number inside the dielectric,

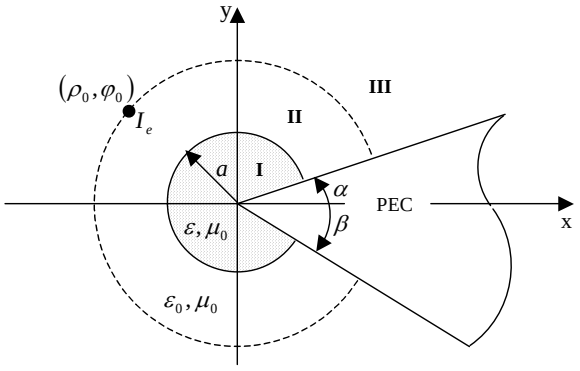

Fig. 3. Capped wedge structure.

$$\nu = \frac{n\pi}{2\pi-\alpha-\beta} \tag{10}$$

while $J_\nu(x)$ and $H_\nu^{(2)}$ are the Bessel and Hankel functions of order ν and argument x. From the Maxwell equations, the magnetic field component H_φ is related to the electric field component E_z for a TM wave by

$$H_\varphi = \frac{1}{j\omega\mu}\frac{\partial E_z}{\partial \rho}. \tag{11}$$

Thus, the magnetic field component H_φ in the various regions may be written as

$$\begin{aligned} H_\varphi^{\mathrm{I}} &= \frac{k_1}{j\omega\mu_0}\sum_{n=0}^{\infty} a_n J_\nu'(k_1\rho)\sin\nu(\varphi-\alpha)\sin\nu(\varphi_0-\alpha), \\ H_\varphi^{\mathrm{II}} &= \frac{k_0}{j\omega\mu_0}\sum_{n=0}^{\infty}\left(b_n J_\nu'(k_0\rho)+c_n H_\nu^{(2)'}(k_0\rho)\right) \\ &\sin\nu(\varphi-\alpha)\sin\nu(\varphi_0-\alpha), \\ H_\varphi^{\mathrm{III}} &= \frac{k_0}{j\omega\mu_0}\sum_{n=0}^{\infty} d_n H_\nu^{(2)'}(k_0\rho)\sin\nu(\varphi-\alpha)\sin\nu(\varphi_0-\alpha), \end{aligned} \tag{12}$$

where the prime indicates derivatives with respect to the full argument of the function. The boundary conditions require that the tangential electric field components vanish at the PEC surface. Also, the tangential field components should be continuous across the air-dielectric surface and the virtual boundary between the regions I and II, except for the discontinuity of the magnetic field at the source point. Thus,

$$E_z = 0 \text{ at } \varphi = \alpha, \quad 2\pi-\beta, \tag{13}$$

$$\begin{cases} E_z^{\mathrm{I}} = E_z^{\mathrm{II}} \\ H_\varphi^{\mathrm{I}} = H_\varphi^{\mathrm{II}} \end{cases} \text{ at } \rho = a, \tag{14}$$

$$\begin{cases} E_z^{\mathrm{II}} = E_z^{\mathrm{III}} \\ H_\varphi^{\mathrm{II}} = H_\varphi^{\mathrm{III}} \end{cases} \text{ at } \rho = \rho_0. \tag{15}$$

The current density J_e may be given in the Fourier series expansion as

$$\begin{aligned} J_e &= \frac{I_e}{\rho_0}\delta(\varphi-\varphi_0) = \frac{2}{2\pi-\alpha-\beta}\ \frac{I_e}{\rho_0}\times \\ &\times\sum_{n=0}^{\infty}\sin\nu(\varphi-\alpha)\sin\nu(\varphi_0-\alpha). \end{aligned} \tag{16}$$

The boundary condition on the PEC surface is automatically satisfied by the φ dependence of the electric field Eq. (9). From the boundary conditions in Eq. (14)

$$\sum_{n=0}^{\infty} a_n J_\nu(k_{1a}) \sin\nu(\varphi-\alpha)\sin\nu(\varphi_0-\alpha) = \\ = \sum_{n=0}^{\infty}\left(b_n J_\nu(k_a)+c_n H_\nu^{(2)}(k_a)\right)\sin\nu(\varphi-\alpha)\sin\nu(\varphi_0-\alpha), \tag{17}$$

$$\frac{k_1}{j\omega\mu_0}\sum_{n=0}^{\infty} a_n J_\nu'(k_{1a})\sin\nu(\varphi-\alpha)\sin\nu(\varphi_0-\alpha) = \\ \frac{k_0}{j\omega\mu_0}\sum_{n=0}^{\infty}\left(b_n J_\nu'(k_a)+c_n H_\nu^{(2)'}(k_a)\right)\sin\nu(\varphi-\alpha)\sin\nu(\varphi_0-\alpha). \tag{18}$$

From the boundary conditions in Eq. (15), we have

$$\sum_{n=0}^{\infty}\left(b_n J_\nu(k_0\rho_0)+c_n H_\nu^{(2)}(k\rho_0)\right)\sin\nu(\varphi-\alpha)\sin\nu(\varphi_0-\alpha) \\ = \sum_{n=0}^{\infty} d_n H_\nu^{(2)}(k_0\rho_0)\sin\nu(\varphi-\alpha)\sin\nu(\varphi_0-\alpha), \tag{19}$$

$$\frac{k}{j\omega\mu_0}\sum_{n=0}^{\infty}\left(b_n J_\nu'(k_0\rho_0)+c_n H_\nu^{(2)'}(k_0\rho_0)\right)\times \\ \times\sin\nu(\varphi-\alpha)\sin\nu(\varphi_0-\alpha) = \\ = \frac{k}{j\omega\mu_0}\sum_{n=0}^{\infty} d_n H_\nu^{(2)'}(k_0\rho_0)\sin\nu(\varphi-\alpha)\sin\nu(\varphi_0-\alpha) - \\ -\frac{2}{2\pi-\alpha-\beta}\frac{I_e}{\rho_0}\sum_{n=0}^{\infty}\sin\nu(\varphi-\alpha)\sin\nu(\varphi_0-\alpha). \tag{20}$$

Since Eqs (17) and (20) hold for all φ, the series of the left and right hand sides are equal term by term, more precisely,

$$a_n J_\nu(k_{1a}) = b_n J_\nu(k_a)+c_n H_\nu^{(2)}(k_a), \tag{21}$$

$$k_1 a_n J_\nu'(k_{1a}) = k\left(b_n J_\nu'(k_a)+c_n H_\nu^{(2)'}(k_a)\right), \tag{22}$$

$$b_n J_\nu(k_0\rho_0)+c_n H_\nu^{(2)}(k_0\rho_0) = d_n H_\nu^{(2)}(k_0\rho_0), \tag{23}$$

$$b_n J_\nu'(k\rho_0)+c_n H_\nu^{(2)'}(k\rho_0) = \\ = d_n H_\nu^{(2)'}(k\rho_0)-\frac{2j\eta_0}{2\pi-\alpha-\beta}\frac{I_e}{\rho_0}, \tag{24}$$

where η_0 is the characteristic impedance of free space.

From Eqs (21) and (23), we have

$$a_n = \frac{1}{J_\nu(k_{1a})}\left[b_n J_\nu(k_a)+c_n H_\nu^{(2)}(k_a)\right], \tag{25}$$

$$d_n = c_n + b_n\frac{J_\nu(k_0\rho_0)}{H_\nu^{(2)}(k_0\rho_0)}. \tag{26}$$

After some mathematical operations, we get

$$b_n = -\frac{\pi\omega\mu_0 I_e}{2\pi-\alpha-\beta}H_\nu^{(2)}(k_0\rho_0). \tag{27}$$

Substituting b_n in Eqs (21) and (22) and solving for c_n yield

$$c_n = \frac{\pi\omega\mu_0 I_e}{2\pi-\alpha-\beta}\times \\ \times\left[H_\nu^{(2)}(k_0\rho_0)\frac{k J_\nu'(k_a)J_\nu(k_{1a})-k_1 J_\nu(ka)J_\nu'(k_{1a})}{k_0 H_\nu^{(2)'}(k_a)J_\nu(k_{1a})-k_1 H_\nu^{(2)}(k_a)J_\nu'(k_{1a})}\right]. \tag{28}$$

From Eqs (26) through (28), d_n may be given by

$$d_n = \frac{\pi\omega\mu_0 I_e}{2\pi-\alpha-\beta}\times \\ \times\left[H_\nu^{(2)}(k_0\rho_0)\frac{k_0 J_\nu'(k_a)J_\nu(k_{1a})-k_1 J_\nu(k_a)J_\nu'(k_{1a})}{kH_\nu^{(2)'}(k_a)J_\nu(k_{1a})-k_1 H_\nu^{(2)}(k_a)J_\nu'(k_{1a})}-\right. \\ \left.-J_\nu(k_0\rho_0)\right] \tag{29}$$

with these closed form expressions for the expansion coefficients a_n, b_n, c_n and d_n, the field components E_z and H_φ can be determined from Eqs (9) and (12), respectively. Alternatively, the magnetic field component H_ρ can be computed from

$$H_\rho = -\frac{1}{j\omega\mu}\frac{1}{\rho}\frac{\partial E_z}{\partial\varphi}. \tag{30}$$

Thus, the H_ρ expressions for the three regions defined in Fig. 3 become

$$H_\rho^{\mathrm{I}} = -\frac{1}{j\omega\mu\rho}\times \\ \times\sum_{n=0}^{\infty} a_n\nu J_\nu(k_1\rho)\cos\nu(\varphi-\alpha)\sin\nu(\varphi_0-\alpha), \\ H_\rho^{\mathrm{II}} = -\frac{1}{j\omega\mu\rho}\times \\ \times\sum_{n=0}^{\infty}\nu\left(b_n J_\nu(k_0\rho)+c_n H_\nu^{(2)}(k_0\rho)\right)\cos\nu(\varphi-\alpha)\sin\nu(\varphi_0-\alpha), \\ H_\rho^{\mathrm{III}} = -\frac{1}{j\omega\mu\rho}\times \\ \times\sum_{n=0}^{\infty} d_n\nu H_\nu^{(2)}(k_0\rho)\cos\nu(\varphi-\alpha)\sin\nu(\varphi_0-\alpha). \tag{31}$$

In the region III, the far scattered field may be found as the difference between the total and incident field. Thus, using Eqs (8) and (9) and considering the far-field condition $(\rho\to\infty)$ we get

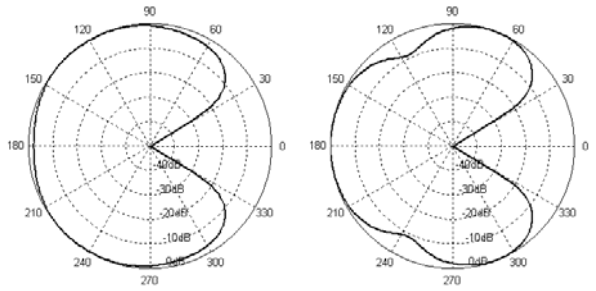

Fig. 4. Total far-field pattern of a line source near a conducting wedge with conducting-capped (a) and dielectric-capped edges (b).

$$E_z^{\mathrm{III}} = E_z^i + E_z^s = \sqrt{\frac{2j}{\pi k_0 \rho}} e^{-jk\rho} \times \times \sum_{n=0}^{\infty} d_n j^{\nu} \sin\nu(\varphi - \alpha) \sin\nu(\varphi_0 - \alpha). \quad (32)$$

For the plane wave excitation $(\rho_0 \to \infty)$, the expressions in Eqs (27) and (28) reduce to

$$b_n = -\frac{\pi \omega \mu_0 I_e}{2\pi - \alpha - \beta} j^{\nu} \sqrt{\frac{2j}{\pi k_0 \rho_0}} e^{-jk_0\rho_0}, \quad (33)$$

$$c_n = \frac{\pi \omega \mu_0 I_e}{2\pi - \alpha - \beta} j^{\nu} \sqrt{\frac{2j}{\pi k_0 \rho_0}} e^{-jk_0\rho_0} \times \times \frac{k_0 J_{\nu}'(k_a) J_{\nu}(k_{1a}) - k_1 J_{\nu}(k_a) J_{\nu}'(k_{1a})}{k_0 H_{\nu}^{(2)'}(k_a) J_{\nu}(k_{1a}) - k_1 H_{\nu}^{(2)}(k_a) J_{\nu}'(k_{1a})}, \quad (34)$$

where the complex of the incident plane wave, E_0, can be given by

$$E_0 = -I_e \frac{\omega \mu_0}{4} \sqrt{\frac{2j}{\pi k \rho_0}} e^{-jk_0\rho_0} \quad (35)$$

in this case, the field components can be evaluated in the regions I and II only.

3. Numerical results and discussion

Fig. 2 presents the radar cross section of a rectangular flat plate for the vertical and horizontal polarizations, compared with the classical formulae. The parameters of structure are $a = b = 10.16$ cm and $f = 300$ MHz.

Fig. 4 presents the far-field of a capped wedge in the presence of an electric line source field. We clearly show how the cap parameters affect the maximum radiation of the line source in the presence of wedge. The distribution of the components of the fields on the near-field of two cases (conducting capped edge, dielectric capped edge) is computed and shown in Figs 5 and 6. The near-field distribution for an incident wave field of these two types of wedges is also computed and shown in Figs 7 and 8. These near-field distributions clearly demonstrated the effect of cap parameters in altering the sharp edge singular behaviour. We have used the following wedge structure parameters: a= 0.15 cm, ρ_0 = 0.5 cm, $\alpha = \beta = 30^\circ$, ε_γ = 3, I_e = 1 mA.

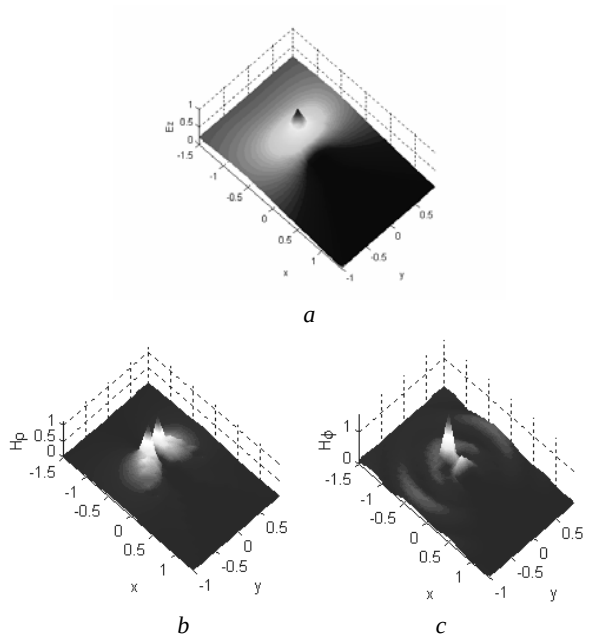

Fig. 5. Near-field patterns of a line source near a conducting wedge with a conducting-capped edge E_z (a), H_ρ (b), H_φ (c).

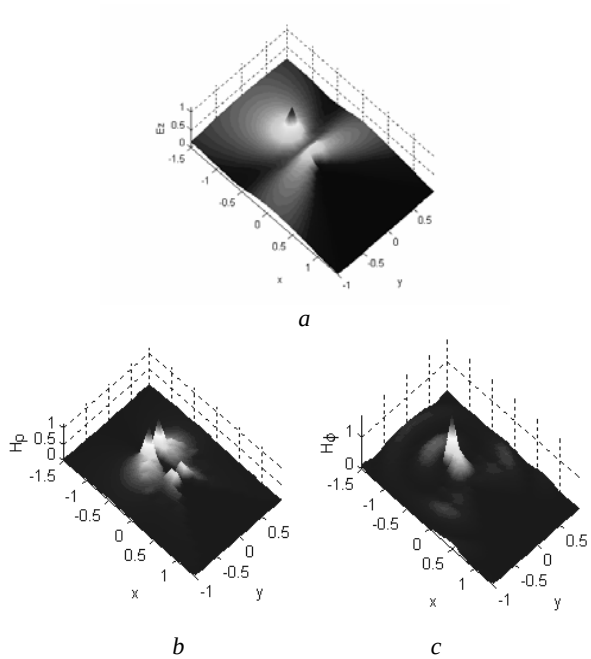

Fig. 6. Near-field patterns of a line source near a conducting wedge with a dielectric-capped edge E_z (a), H_ρ (b), H_φ (c).

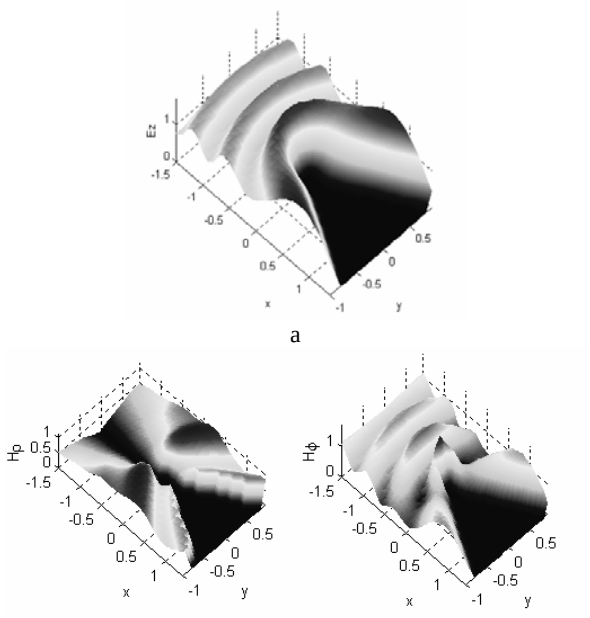

a

b c

Fig. 7. Near-field patterns of the plane wave incident on a conducting wedge with a conducting-capped edge E_z (a), H_ρ (b), H_φ (c).

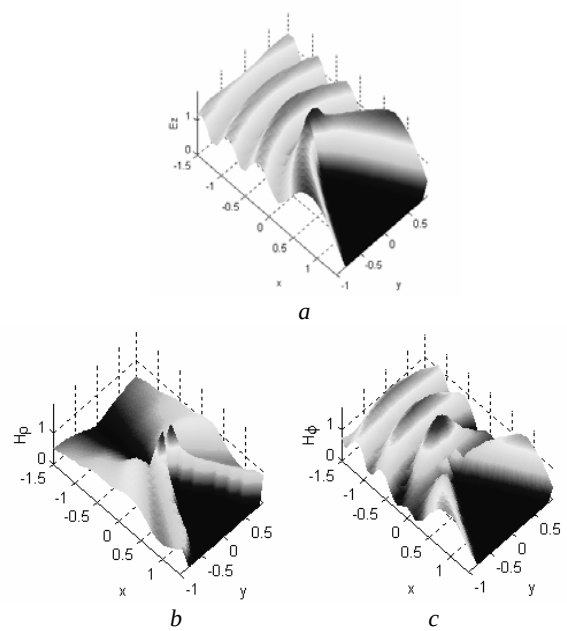

a

b *c*

Fig. 8. Near-field patterns of the plane wave incident on a conducting wedge with a dielectric-capped edge E_z (a), H_ρ (b), H_φ (c).

4. Conclusion

In this paper, we have presented a full analysis of electromagnetic scattering. We have presented a case of backscattered radar cross section for a rectangular flat plate. The analysis of the far- and near-field patterns for a wedge structure shows the effect of cap parameters on the maximum radiation of the line source. We have also examined the effect the cap parameters on the sharp edge behavior for an incident plane wave.

References

1. S.K. Jeng, Near-field scattering by physical theory of diffraction and shooting and bouncing rays // *IEEE Trans. Ant. Propag.* **46**(4), p. 551-558 (1998).
2. N.N. Youssef, Radar cross section of complex targets // *Proc. IEEE* **77**(5), p. 722-734 (1989).
3. D. Colton and R. Kress, *Integral equation methods in scattering theory*. Wiley-Interscience, 1983.
4. R.G. Kouyoumjian and P.H. Pathak, A uniform geometrical theory of diffraction for an edge in a perfectly conducting surface // *Proc. IEEE*, **62**(11), p. 1448-1461 (1974).
5. S.M. Rao, D.R. Wilton, and A.W. Glisson, Electromagnetic scattering by surfaces of arbitrary shape // *IEEE Trans. Ant. Propag.* **AP-30**(3), p. 409–418 (1982).
6. E.F. Knott, J.F. Shaeffer and M.T Tuley, *Radar cross section: Its prediction, measurement and reduction*. Artech House, Dedham, MA, 1985.
7. S. Blume and V. Krebs, Numerical evaluation of dyadic diffraction coefficients and bistatic radar cross sections for a perfectly conducting semi-infinite elliptic cone // *IEEE Trans. Ant. Propag.* **46**(3), p. 414– 424 (1998).
8. C.A. Balanis, *Antenna theory: Analysis and design*. John Wiley & Sons, 2nd edition, New York, 1997.
9. R.A Ross, Radar cross section of rectangular flat plate as function of aspect angle // *IEEE Trans. Ant. Propag.* **AP-14**, p. 329-335 (1966).